A substitution method for nanoscale capacitance calibration using scanning microwave microscopy

OPEN ACCESS
IOP Publishing
Measurement Science and Technology
Meas. Sci. Technol. **31** (2020) 074009 (10pp)
https://doi.org/10.1088/1361-6501/ab82c1

A substitution method for nanoscale capacitance calibration using scanning microwave microscopy

José A Morán-Meza, Alexandra Delvallée, Djamel Allal and François Piquemal

Laboratoire National de métrologie et d'Essais (LNE), 29 Avenue Roger Hennequin 78197, Trappes Cedex, France

E-mail: francois.piquemal@lne.fr

Received 20 December 2019, revised 17 March 2020
Accepted for publication 24 March 2020
Published 30 April 2020

Abstract

This paper presents a calibration method and an uncertainty budget for capacitance measurements performed on micrometric size capacitors at microwave frequencies and nanometric resolution using a scanning microwave microscopy (SMM). The method applies the classical one-port vector network analyzer calibration for SMM using three known capacitance standards. These standards are established from a commercial calibration kit placed close to the microcapacitors in order to be calibrated. The calibration kit is composed of a large number of Metal-Oxide-Semiconductor (MOS) microcapacitors with capacitance values C ranging from 0.1 fF to 8.6 fF. Diligent selection criteria were established for the choice of the three capacitors. Their capacitance values were calculated from the AFM measured values of the area of the top electrodes and the dielectric thickness and considering the contribution of fringing fields. The combined type uncertainty on these calculated values amounts between 5% and 14% in relative value (uncertainty given at one standard deviation). The comparison between the capacitance values measured on calibration kit capacitors using the calibrated SMM and the calculated values show a good agreement for capacitances higher than 0.8 fF within uncertainties varying between 6% and 9%. For smaller capacitances, most of the observed deviations are not significant at two standard deviations. The uncertainties are mostly dominated by dimensional measurements and less importantly by unwanted capacitance effects. Based on these results, capacitances of two sets of microcapacitors were calibrated. The combined uncertainties vary from 14% to 7% for capacitances ranging from 0.1 fF to 3.1 fF respectively. The permittivity values of the dielectric layer of the two samples have been determined. They are found equal to 4.0 and 4.1 with a standard uncertainty of 0.6 and correlate with the expected value of 3.9.

Keywords: scanning microwave microscopy, calibration kit, calibration method, nanoscale capacitance measurements, Metal-Oxide-Semiconductor (MOS), microcapacitor, uncertainty

(Some figures may appear in colour only in the online journal)

1. Introduction

Currently, the development of electronics and the continuous miniaturisation of electronic components (transistors, resistors, and capacitors [1]) has proceeded to the point where many components have now attained sub-10 nm dimensions

[2]. At this small scale, the electrical properties like other physical properties (magnetic, thermal, optical…) differ substantially from the bulk behavior and making their nanoscale measurements accurate, reliable and comparable is a real challenge for metrology. Consideration ought to be given towards the traceability of nanoscale impedance measurements currently performed on nano-structured surfaces, nanodevices or nanomaterials. This metrological issue is becoming critical in a number of industries such as consumer electronics, healthcare, security and energy devices [3]. Among various nanoscale circuit elements, nanoscale capacitors have attracted great interest in nanoelectronics for advanced energy storage technology [4]. High density three-dimensional nanocapacitor arrays have been intensively studied due to increasing demands of high capacity, lightweight, and compact energy storage devices [4–6]. Nanoscale capacitors also have been used as building blocks in memory technology [4, 7, 8].

Current methods for measuring capacitance at the nanoscale remain challenging due to the small feature size and their sub-femtofarad capacitance values. One of them involves a non-destructive quantitative characterization tool, the scanning microwave microscopy (SMM). This technique has been developed to measure local electrical properties such as impedance [9], capacitance [10–12], dopant concentration [13, 14], and electrical permittivity [9, 15] of materials at microwave frequencies.

To date, several works on nanoscale capacitance measurements by SMM have been reported [9, 16–22]. Few of them have provided an uncertainty estimation by doing some asumptions [11] or have identified measurement errors with relative values higher than 10% [10, 12, 18]. Unfortunately no comprehensive uncertainty budget has been established yet, including particularly details on the uncertainties due to the dimensional measurements from which the SMM capacitance measurements are traceable to the SI. Moreover no repeatability or reproducibility on these published capacitance measurements has been indicated. Last but not least, to our knowledge, no results have been reported about calibrated capacitance measurements based on Short Open Load (SOL) method, carried out on capacitors other than those used as reference to calibrate the SMM.

The main purpose of this work is to provide SMM users with a calibration method allowing them both to carry out quantitative nanoscale capacitance measurements on micrometric size capacitors and to estimate the associated uncertainties, including repeatability and dimensionnal measurements. This can be considered as a first step towards developing metrology for local capacitance measurements on nanometric size capacitors and in the sub femtofarad range [23].

In the following sections, we give a general description of the SMM set-up recently implemented at LNE and the SMM calibration method involving the selection of capacitance standards from a calibration kit. Then, in a first step we present at first the results about SMM calibration based on selected capacitance standards and SMM measurements carried out on a set of capacitors from the same calibration kit. In a second step, we report for the first time the capacitance calibration results on 'unknown' microcapacitors by substitution method. The main contributions to the uncertainty budgets drawn up for SMM calibration and capacitance measurements are discussed.

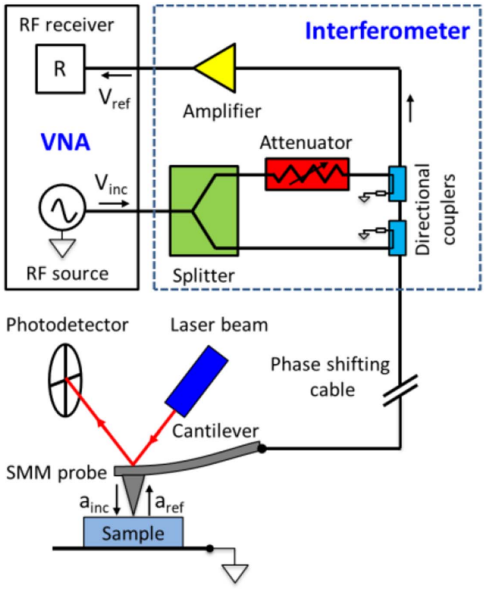

Figure 1. Schematic diagram of the interferometric SMM setup, showing the AFM interfaced with VNA.

2. Experimental section

2.1. SMM principle

SMM consists of an atomic force microscope (AFM) interfaced with a vector network analyzer (VNA) operating at GHz frequencies. The conductive AFM tip is connected to the MW source/meter of VNA (figure 1). While the tip scans over the sample surface in conventional AFM imaging modes, the tip irradiates the microwave signal over a local region on the sample, allowing simultaneous topographic and electrical characterization of the sample. Depending on the mismatch between the characteristic impedance (Z_0) and the local impedance of the tip-sample system (Z_s), part of the incident signal is reflected back travelling from the tip-sample contact point to the VNA and part is transmitted throughout the sample. The ratio between the reflected and incident signals, the so-called S_{11} scattering parameter, is then measured by the VNA and converted into complex impedance values following the one-port VNA calibration procedure [11].

2.2. SMM setup

The SMM system used in this work consists of a commercial 5600LS AFM interfaced with a N5230C VNA (both from Keysight Technologies). [1]

[1] Commercial instruments are identified in this paper in order to adequately specify the experimental setup and do not imply recommendation or endorsement by the authors.

2.2.1. Environmental conditions. The SMM microscope is installed in a MBraun Inert Gas System glove box under a nitrogen atmosphere at room temperature (T = 24.3°C ± 0.1°C) to carry out SMM measurements in dry conditions (RH < 1%) and in order to reduce the parasitic capacitance contribution arising from the water meniscus formed at the point of contact between the SMM tip and the sample surface. The whole set-up is placed in a shielded room to minimize interfering electromagnetic signals from surroundings.

2.2.2. Mach Zehnder configuration of SMM. The VNA operates from 0.5 GHz to 6.0 GHz with intermediate frequency (IF) bandwidth of 1 kHz. The SMM integrates a microwave interferometer based on a Mach–Zehnder configuration [12, 24] (figure 1).

This adjustable interferometric SMM system combines three advantages compared to the standard SMM setup showing a better signal-to-noise ratio, a wide range of measurable impedances, and various working frequencies with impedance-matching notches relatively deeper [12, 24]. For more details about the Mach Zehnder SMM configuration, the reader could refer to [12].

2.2.3. Imaging conditions. SMM images were acquired in contact mode at a frequency of 3.8086 GHz with imaging rates of 15 min at 512 × 512 pixels. SMM imaging includes AFM topography simoultanously performed with $S_{11,m}$-Magnitude and $S_{11,m}$-Phase maps.

Solid platinum tips (25Pt300A) from Rocky Mountains Nanotechnology were used for SMM measurements, having a standard tip radii below 20 nm. The SMM is placed on an active anti-vibration table to reduce external mechanical vibrations during surface closed-loop scanning.

2.2.4. Choice of the VNA operating frequency. Before landing the SMM probe on the sample surface, the probe is moved 20 μm above the substrate surface and a full frequency sweep of VNA signal is performed over its frequency range. The microwave frequency minimizing the $S_{11,m}$—Magnitude signal is chosen (figure 2).

173 working frequencies have been found, the interference occuring each one 31.6 MHz. 16 of them match to peaks with a quality factor Q higher than 10^4. With the selected frequency, $f = 3.808\,6$ GHz, Q reaches the highest value of $1.7 \cdot 10^6$ thus maximizing the SMM sensitivity.

2.2.5. SMM dimensional calibration. To perform accurate 3D topography maps, the AFM system was dimensionally calibrated using a surface topography standard STS2-440P from VLSI Standards with a pitch of (1807 ± 11.5 nm) and a height of (42.1 ± 0.35) nm. This uncertainty like all those mentioned in the paper is given at one standard deviation corresponding to a 68% confidence level in the case of a normal distribution [26]. Gwyddion [27] software has been used for the topographic image processing.

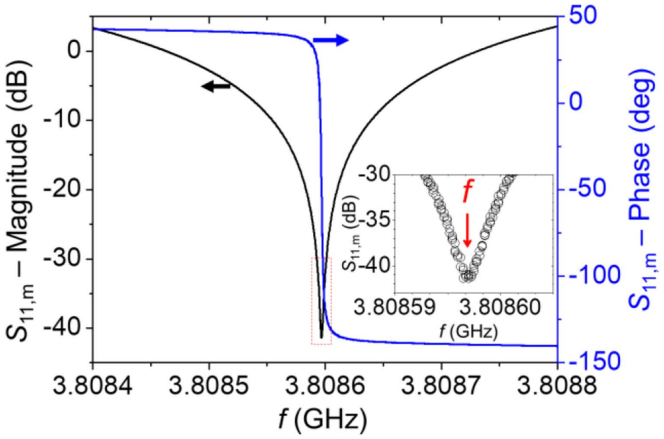

Figure 2. $S_{11,m}$—Magnitude and $S_{11,m}$—Phase vs. frequency. Zoom-in of a deep notch at $f = 3.8086$ GHz (4096 points).

2.3. SMM calibration method

To perform quantitative impedance measurements (capacitance measurements in this work), a first fundamental step is the calibration of the SMM with the aim at converting the raw measured reflection coefficient $S_{11,m}$ into the complex impedance of the sample under study Z_s. To this end, the modified Short Open Load (SOL) calibration method proposed by Hoffmann *et al* [11] and Dargent *et al* [12] is used. The quantities $S_{11,m}$ and Z_s are related by two equations:

$$S_{11} = \frac{Z_s - Z_0}{Z_s + Z_0} \tag{1}$$

$$S_{11,m} = e_{00} + e_{01}\left(\frac{S_{11}}{1 - e_{11}S_{11}}\right) \tag{2}$$

where S_{11} is the expected reflection coefficient and e_{00}, e_{01}, and e_{11} are three complex parameters (also known as error parameters) to be determined from $S_{11,m}$ measurements on three reference structures with known impedances values.

2.3.1. Calibration kit. A commercial calibration kit fabricated by MC2 Technologies [28] is used to calibrate the SMM. It consists of 144 identical patterns and each pattern includes four 48 MOS capacitors with capacitance values ranging from 100 aF to 10 fF typically, depending on the size dimensions and the dielectrical material (figure 3). The MOS capacitors consist in circular gold electrodes deposited on silicon dioxide with different thicknesses and a highly bore doped p-type Si (100) substrate forming a back electrode. The doping concentration N_a ($= 7.98 \cdot 10^{18}$ atoms cm^{-3}) was calculated from the electrical resistivity ρ ($= 0.01$ Ω.cm) given by the manufacturer. The diameters of the gold electrodes are 1 μm, 2 μm, 3 μm and 4 μm. The thicknesses of the SiO_2 layers range from 50 nm to 220 nm with about 50 nm steps. More details about the fabrication process of calibration sample are described elsewhere [10, 28].

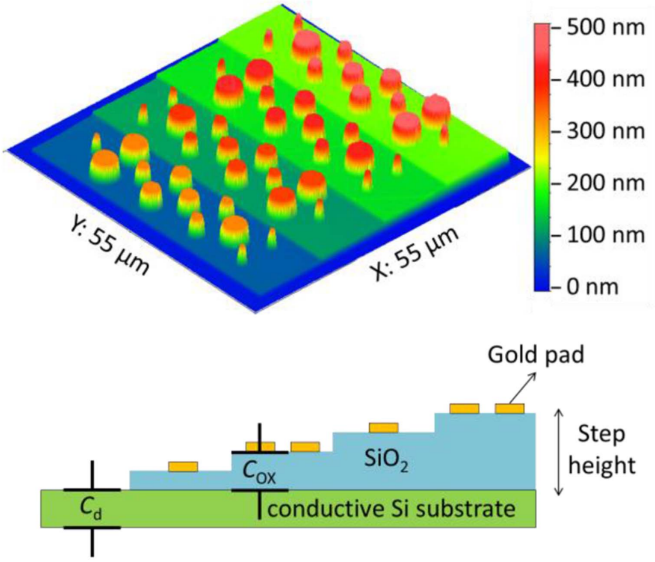

Figure 3. AFM topography of the calibration kit and capacitance model.

2.3.2. Electrical model of the capacitors. The capacitance C of each MOS capacitor of the calibration kit is modeled as the capacitance of two capacitors connected in series (figure 3). The first capacitor of capacitance C_{ox} consists of a circular plate capacitor with a top electrode of finite size radius R, separate by a dielectric layer of relative permittivity ε_r and a thickness d from the back electrode considered as an infinite plan, since its equivalent radius is nearly 100 times larger than the largest R (2 µm). The second capacitor has a capacitance C_d due to a depletion layer occurring inside the highly doped Si substrate which composes the back electrode. Thus, the capacitance C is given by:

$$C = \frac{C_d \cdot C_{ox}}{C_d + C_{ox}}. \tag{3}$$

The capacitance C_{ox} was calculated by finite element modeling (FEM) using COMSOL Multiphysics 5.3 to take into consideration the fringing fields [12]. We have used a 2D axisymmetric model, which is faster and more accurate than 3D calculations. The top and back plane electrodes of each circular capacitor were set to 1 V and 0 V, respectively. The top and right boundaries of the simulation box were set to 0 V, while the left boundary represents the symmetry axis. The simulation box dimensions used for the model are: $L_{box,x} = R + 10\,d$, $L_{box,y} = 5\,d$. The thickness and radius of the dielectric environment were set to d and $L_{box,x}$, respectively. The $\varepsilon_{r,ox}$ was set to 3.9 for silicon dioxide [29, 30] and the global meshing quality was set to 'extremely fine'.

On the other hand, the depletion capacitance C_d is given by the relation [31]:

$$C_d = \pi \varepsilon_{r,Si}\, \varepsilon_0 \frac{R^2}{l_D}, \tag{4}$$

and depends on the area of the top electrode. In this relation, $\varepsilon_{r,Si}$ is the relative permittivity of the highly doped Si substrate and l_D is the Debye length:

$$l_D = \sqrt{\frac{kT\varepsilon_{r,Si}\,\varepsilon_0}{e^2 N_a}}, \tag{5}$$

where k denotes the Boltzmann constant, T the temperature of the substrate, e the elementary charge and N_a is the dopant concentration of Si substrate. Let us note that the exact values of k and e that are two defining constants in the revised international system of units (SI) can be found in [32].

The choice of the calibration kit with a very high N_a value approaching $8 \cdot 10^{18}$ atoms cm^{-3} makes the C_d capacitance contribution negligible in respect with the dielectric layer C_{ox} capacitance. From (3) in the first approximation order, C is then given by

$$C \approx C_{ox} \cdot (1 - C_{ox}/C_d), \tag{6}$$

with C_{ox}/C_d ratio in the order of $2 \cdot 10^{-4}$ for the calibration kit capacitances.

To estimate the uncertainty on the calculation of C_{ox}, we have used the analytical expression of C_{ox} in terms of $\varepsilon_{r,ox}$, R and d proposed by Sloggett *et al* [33]. This expression was found relevant even for small ratios R/d (going down to 2). In a first order approximation C_{ox} is given by:

$$\frac{C_{ox}}{C_p} \approx 1 + \frac{2d}{\pi R}\left[\ln\left(\frac{8\pi R}{d}\right) - 1\right] + \left[\frac{d}{\pi R}\ln\left(\frac{d}{8\pi R}\right)\right]^2. \tag{7}$$

C_p is the well-known capacitance of the circular plate capacitor calculated from the uniform field model:

$$C_p = \pi \varepsilon_{r,ox}\, \varepsilon_0 \frac{R^2}{d}, \tag{8}$$

where ε_0 is the vacuum electric permittivity [2], $\varepsilon_0 = 8.854\,187\,8128(13)$ pF m^{-1} [34]. The two calculation methods used for C_{ox} show a relative difference $(C_{FEM}—C_{anal})/C_{FEM}$ changing from—26% to 0% for a ratio R/d varying from 2 to 40. This deviation is due to the assumption of a capacitor with a top electrode surrounded by the same dielectric environment in the case of analytical method.

2.3.3. Selection criteria. The calibration procedure for SMM needs at least three reference structures with known impedances values. A poor and arbitrary selection of these three capacitors without established criteria can lead to obtain erroneous results on capacitance measurements after SMM calibration. The three capacitors are selected according to the following criteria:

(i) they present a really clean surface confirmed by AFM;
(ii) they insure a good and homogeneous electrical contact between the SMM tip and their top electrode;
(iii) their capacitances satisfy approximately the inequality $|C_i - C_j| \geqslant \Delta C_{max}/2$,

[2] The number inside brackets indicates the absolute uncertainty. That amounts to a relative uncertainty of 1.5 parts in 10^{10}.

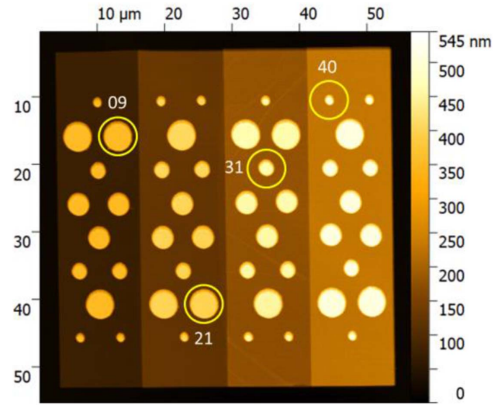

Figure 4. Localisation of particular capacitors in the calibration kit pattern used to calibrate the SMM. (AFM topography).

where i and j (≠i) ranging from 1 to 48 and ΔC_{max} is the difference between the highest and lowest capacitance values.

For the calibration kit used in this work, $\Delta C_{max} = 8.4$ fF and 27 triplets of capacitors fulfill the criteria. Among them, two triplets (C_{09}, C_{21}, C_{31}) and (C_{09}, C_{21}, C_{40}) have been investigated as potential standards. The corresponding capacitors are located on the 4 different terraces (figure 4). They have the following nominal capacitances:

$$C_{09} = 8.6\,\text{fF}, C_{21} = 4.4\,\text{fF}, C_{31} = 0.8\,\text{fF}, C_{40} = 0.2\,\text{fF}. \quad (9)$$

With respect to the triplet (C_{09}, C_{21}, C_{31}), the triplet (C_{09}, C_{21}, C_{40}) presents the advantage to extend the calibration range of the SMM down to sub-femtofarad.

2.3.4. Image processing. During SMM scanning, a linear drift was observed from the raw $S_{11,m}$ data (Magnitude and Phase) in the slow scan Y-direction. Similar drifts were also reported elsewhere [18, 22]. The drift can result from the non-null synchronization time interval between VNA measurements and the AFM topography, both acquired line by line. The drift could also be due to the thermal expansion characteristics of interconnecting cables within the test set.

To get rid of this drift, the raw $S_{11,m}$ images have been processed by taking into account instead the raw data of measurements of the difference $\Delta S_{11,m} = S^{C}_{11,m} - S^{Si}_{11,m}$ by subtracting the raw $S^{Si}_{11,m}$ signals measured on Si substrate from the raw $S^{C}_{11,m}$ signals measured on individual capacitors, line by line. This image processing on raw $S_{11,m}$ maps has also the advantage to null or at least make negligible the errors due to parasitic capacitors occurring in parallel to the microcapacitors under study, such as capacitor between unshielded parts of the SMM and the Si substrate.

For this purpose, a custom MATLAB script (Mathworks Inc.) has been developed to extract the mean value of $\Delta S_{11,m}$ from $\Delta S_{11,m}$-Magnitude and $\Delta S_{11,m}$-Phase histograms that are obtained on each capacitor.

Table 1. Calculated capacitances C_{calc} and measured top electrode area A and thickness d, of four capacitors with standard uncertainties.

Capacitor	C_{calc} (fF)	A (µm × µm)	d (nm)
C_{09}	8.57 ± 0.44	12.64 ± 0.28	55.8 ± 2.5
C_{21}	4.42 ± 0.24	12.03 ± 0.28	106.1 ± 5.0
C_{31}	0.82 ± 0.05	2.98 ± 0.15	159.4 ± 5.7
C_{40}	0.18 ± 0.03	0.65 ± 0.09	212.0 ± 3.8

Table 2. Main uncertainty contributions for the calculation of the selected capacitance standards.

Uncertainty budget for C_i calculation	C_{09}	C_{21}	C_{31}	C_{40}
	(%)			
Area measurements, u_A	2.4	2.5	5.3	14.3
Repeatability	*0.4*	*0.5*	*0.7*	*1.3*
Pitch AFM calibration	*0.9*	*0.9*	*0.9*	*0.9*
Tip profile	*2.2*	*2.3*	*5.2*	*14.2*
Thickness measurements, u_d	4.4	4.7	3.6	1.8
Repeatability	*4.3*	*4.6*	*3.5*	*1.6*
Height AFM calibration	*1.0*	*1.0*	*1.0*	*1.0*
Depletion capacitance, u_{Cd}	0.03	0.02	0.01	0.02
Permittivity ε_r (SiO_2), $u_{\varepsilon r}$	1	1	1	1
Combined uncertainty u_C	5.1	5.4	6.5	14.4

3. Results and discussion

3.1. SMM calibration for capacitance measurements

3.1.1. Calculated capacitance of selected capacitors The calculated capacitance values C_{calc} of the four selected capacitors are given in table 1. The reported values of the top electrode area A and the SiO_2 layer thickness d have been measured from a series of 15 topography images.

The standard uncertainties corresponding to the calculated capacitances and to the area and thickness measurements result from the main uncertainty contributions that are summarized in table 2.

The combined uncertainty u_A on the A measurements is given by the root sum square of the standard uncertainties related to the measurement repeatability, the pitch AFM calibration and the tip profile.

The combined uncertainty u_d on the d measurements takes into account two terms, the measurement repeatability and the height AFM calibration. Two other uncertainty contributions can be considered but have a minor impact on the budget. The first is related to the depletion capacitance effect and does not exceed 3 parts in 10^4. The second uncertainty contribution comes from the uncertainty of the relative permittivity of SiO_2 set at 3.9. An uncertainty in the order of 1 part in 10^3 can be reached from split-cylinder cavity techniques [35]. However this uncertainty has not yet been demonstrated in conjunction with SMM measurements. A conservative uncertainty value of 1% is therefore taken into account.

The combined uncertainty u_C on the calculated capacitances, given by the root sum square of u_A, u_d, u_{Cd} and $u_{\varepsilon r}$, varies from 5.1% for the highest capacitance value (8.57 fF)

up to 14.4% for the smallest value (0.18 fF). The uncertainty is largely dominated by the error due to the tip profile in the case of the smallest area capacitor (C_{40}) and the lack of repeatability on the thickness measurements for the three other capacitors.

On the one hand, an uncertainty has to be considered on the correction of A measurements which has been done to take into account the real tip profile (apex radius and cone angle). This uncertainty has been estimated by comparing AFM and scanning electron microscopy (SEM) topography images of micro-capacitors from a very similar calibration kit (same growth batch) to the one used as reference in this work. This uncertainty could be further reduced by fitting the SMM with a thinner tip, carrying out SEM and SMM measurements in a same run [36] or in a simpler way by using a step edge structure. Other improvement axes exist in particular about the design of the calibration kit capacitors (thinner top electrodes…).

On the other hand, the repeatability results on the thickness measurements, although less favorable for thinner dioxide layers, show unexpectedly too high uncertainty for the capacitor C_{21}, and that could be due to a bad levelling process during the image treatment.

Furthermore, it has been found that the optimal number of measurements to minimize the repeatability uncertainty both for area and thickness measurements is around 5. This number results from a compromise between the evolution of standard deviation and instrumental drifts.

3.1.2. Capacitance SMM measurements A series of 15 capacitance measurements have been carried out on all the 48 capacitors of the same calibration kit pattern which includes the standard capacitors C_{09}, C_{21}, C_{31}, and C_{40}. For each measurement (both topographic and electrical), the data were processed twice, by calibrating the SMM separately with the triplets (C_{09}, C_{21}, C_{31}) and (C_{09}, C_{21}, C_{40}).

The two sets of values shown in figures 5 and 6 correspond to the relative deviation $\Delta C_i/C_{calc,i}$ of the measured capacitance $C_{m,i}$ from the calculated capacitance $C_{calc,i}$ for each capacitor C_i, the index i ranging from 1 to 48

$$\frac{\Delta C_i}{C_{calc,i}} = \frac{C_{m,i} - C_{calc,i}}{C_{calc,i}}. \tag{10}$$

Each value is marked by two vertical error bars and one horizontal error bar. The smallest vertical bars reflect the measurement repeatability (standard uncertainty $u_{S,i}$) while the largest vertical bar, $u_{L,i}$ corresponds to the root sum square of the SMM calibration uncertainty $u_{SMM,i}$ and the standard uncertainty $u_{Ccalc,i}$ (indicated by the horizontal error bars) on the calculation of $C_{calc,i}$.

The first term $u_{SMM,i}$ is calculated from the deviation of the dispersion of 27 capacitance values measured on the capacitor C_i by considering the 3 values $C_{calc,j}$, $C_{calc,j} + u_{Ccalc,j}$, and $C_{calc,j} - u_{Ccalc,j}$ for each triplet capacitors used to calibrate the SMM (C_{09}, C_{21}, C_{31} or C_{40}). This is equivalent to the measurement of C_i using 27 capacitance triplets.

As expected, the results show a clear advantage for the standard triplet (C_{09}, C_{21}, C_{40}) over (C_{09}, C_{21}, C_{31}) to be used for measuring capacitances lower than 0.8 fF. The $u_{L,i}$ uncertainty (table 3) is significantly smaller. Most of the observed positive deviations $\Delta C_i/C_{calc,i}$ occur between 0% and 35%. In contrast, when the triplet (C_{09}, C_{21}, C_{31}) is used, the deviations are larger, lying between 30% and around 70%. However, in both cases, these deviations occurred for capacitances smaller than 0.6 fF which correspond to capacitors of smallest area (diameter 1 μm) and could be explained by an error on the area determination. It must be noted that most of these deviations can be considered as non-significant within two standard deviations.

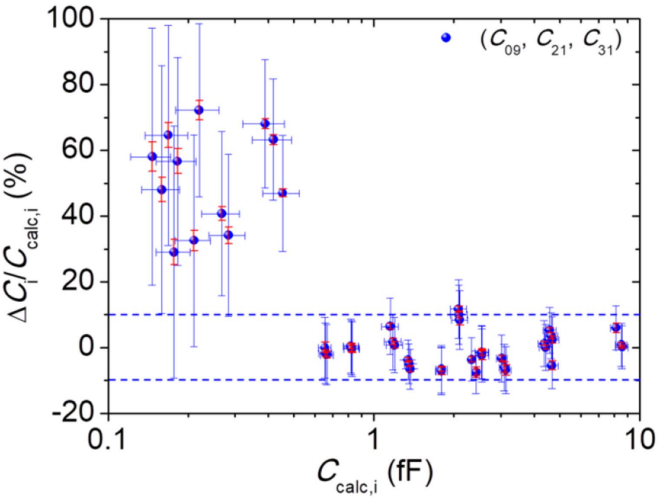

Figure 5. Relative differences $\Delta C_i/C_{calc,i}$ between measured $C_{m,i}$ and calculated $C_{calc,i}$ capacitance values for 48 capacitors C_i by using capacitance standards (C_{09}, C_{21}, C_{31}). The dashed lines indicate the values at ±10%. The vertical bars correspond to the standard uncertainties $u_{S,I}$ (in red) and $u_{L,I}$ (in blue). The horizontal bars correspond to the standard uncertainty $u_{Ccalc,i}$.

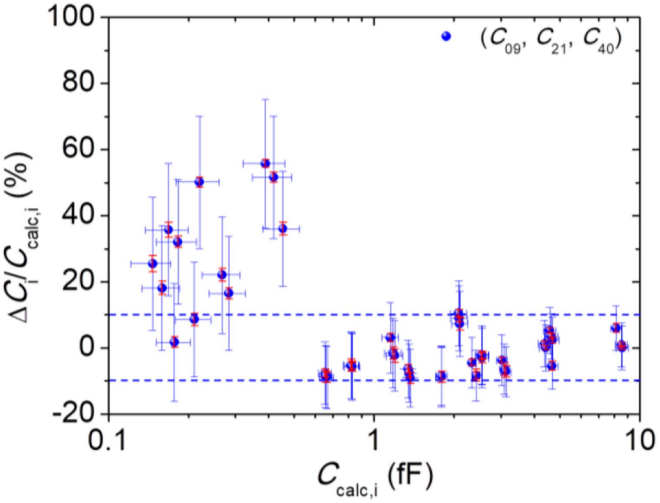

Figure 6. Relative differences $\Delta C_i/C_{calc,i}$ between measured $C_{m,i}$ and calculated $C_{calc,i}$ capacitance values for 48 capacitors C_i by using capacitance standards (C_{09}, C_{21}, C_{40}). The vertical bars correspond to the standard uncertainties $u_{S,I}$ (in red) and $u_{L,I}$ (in blue). The horizontal bars correspond to the standard uncertainty $u_{Ccalc,i}$.

Table 3. Uncertainties (%) on the capacitance measurements using capacitance standard triplets (C_{09}, C_{21}, C_{31}) and (C_{09}, C_{21}, C_{40}).

	$C_i \leqslant 0.8$ fF		$C_i \geqslant 0.8$ fF	
Triplet	09,21,31	09,21,40	09,21,31	09,21,40
u (%)				
$u_{S,i}$	0.9–4.5	1.1–2.5	0.6–1.6	0.6–1.9
$u_{L,i}$	9–39	9–20	6–9	7–11
$u_{SMM,i}$	7–35	7–10	4–7	4–8
$u_{Ccalc,i}$	6–19		3–7	

For capacitances higher than 0.8 fF, a good agreement is found within the $u_{L,i}$ uncertainty independently of the triplet used with a slight advantage for (C_{09}, C_{21}, C_{31}) over (C_{09}, C_{21}, C_{40}). The mean values of the relative deviations $\Delta C_i/C_{calc,i}$ amount to $(-0.8 \pm 5.2)\%$ and $(-2.6 \pm 5.6)\%$ respectively. The repeatability uncertainties are similar in the two cases. Like for topographic images, the repeatability level reaches here its minimum value from 5 measurements upwards.

In addition to the standard uncertainties above-mentioned, other uncertainty contributions should be cited. These uncertainties are due to parasitic effects from stray capacitances.

Because the SMM probe is not fully shielded, unwanted non-local capacitances occurred in parallel to the measured capacitances, between the tip apex and the Si substrate. Considering some dimensional parameters of the system (surface of the unshielded parts: tip and cantilever, distance to the silicon substrate), the unwanted capacitances are estimated in the order of 2.6 fF (capacitance between cantilever and substrate) and 70 aF (capacitance between tip and substrate), following the calculation method in [37]. Since the method adopted here consists in measuring the difference $\Delta S_{11,m} = S^{C}_{11,m} - S^{Si}_{11,m}$ (section 2.3.4), the errors due to stray capacitances are strongly reduced. The calculated residual error varies from –3 aF to –12 aF in function of the dielectric layer thickness, 56 nm–212 nm respectively.

Another unwanted capacitances come from the water meniscus occurring in series between the tip apex and the imaged surface (top electrode of the capacitor and Si substrate). The inert gas environment insured by the glove box limits this parasitic effect but does not cancel it out. The $\Delta S_{11,m}$ measurement does not allow us to eliminate the water meniscus effect because of the different hydrophobic or hydrophilic behavior between Au and Si materials. Based on some estimates of water meniscus capacitance surrounding the SMM tip, found in the order of aF [18], the expected error here should not exceed 10 aF.

If all these stray capacitances are not zeroed, they are at least stable enough in space and in time. This is a crucial point because of the requirement to preserve a constant calibration plan which is at the level of the tip where the electrical connections of the three standards are placed [9]. A first indication of stability is given by the good level of repeatability measured on a single pattern, in the order of 1% typically or 10 aF for 1 fF (table 3). Moreover, no discrepancy has been observed

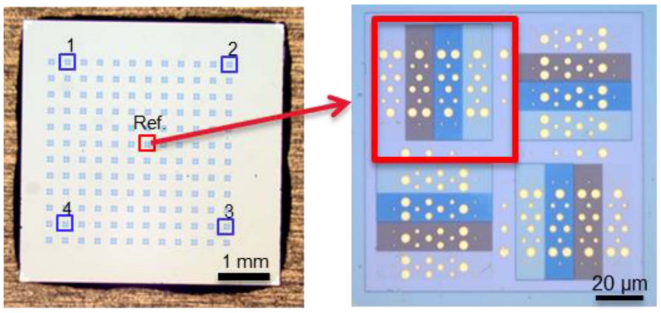

Figure 7. Localization of 5 measured patterns on calibration kit. In the centre, the pattern used as reference (labelled Ref).

Table 4. Root mean square deviations $\delta C_{rms,k}$ of capacitances measured on 5 patterns of calibration kit.

Order of measurement	Pattern	$\delta C_{rms,k}$ (aF)
1 (start)	M_{Ref}	79
2	M_1	84
3	M_2	74
4	M_3	71
5	M_4	105
6 (end)	M_{Ref}	77

from capacitances measured on 5 different patterns of the calibration kit including the pattern which contains the capacitors C_{09}, C_{21}, C_{31}, and C_{40} (figure 7).

Let us consider the root mean square deviation $\delta C_{rms,k}$ calculated for each pattern Mk

$$\delta C_{rms,\,k} = \sqrt{\frac{1}{48}\sum_{i=1}^{48}\left(C_{m,i,k} - C_{calc,i,Ref}\right)^2}, \qquad (11)$$

where $C_{m,i,k}$ denotes the measured capacitance of the ith capacitor of kth pattern (k from 1 to 4 and ref) and $C_{calc,i,Ref}$ is the calculated capacitance of the ith capacitor of the reference pattern. The $\delta C_{rms,k}$ values do not differ significantly from the two $\delta C_{rms,Ref}$ values measured on the reference pattern within a standard deviation of 15 aF (table 4).

3.2. Capacitance calibration on 'unknown' capacitors

Based on the stability of the parasitic effects due to stray capacitances as previously shown, the SMM can be used to calibrate capacitances of microcapacitors which are placed in the vicinity of the reference calibration kit so that the SMM calibration using the capacitor triplet (C_{09}, C_{21}, C_{40}) is preserved. To demonstrate this possibility, two calibration kits from MC2 Technologies have provided the 'unknown' capacitances. These kits, labelled M57 and M58, have same number of patterns and capacitors with similar organization (four SiO_2 dielectric terraces of different thickness …) but came from different growth batches and not based on the same doped Si substrate.

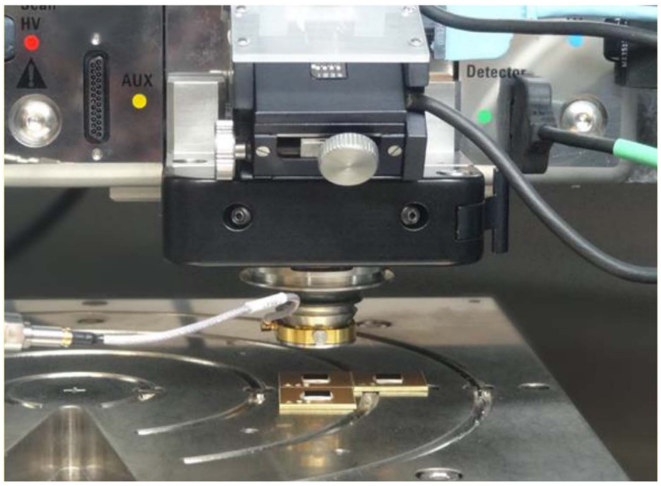

Figure 8. Reference calibration kit (in the centre) and two samples (M57, M58) to be calibrated.

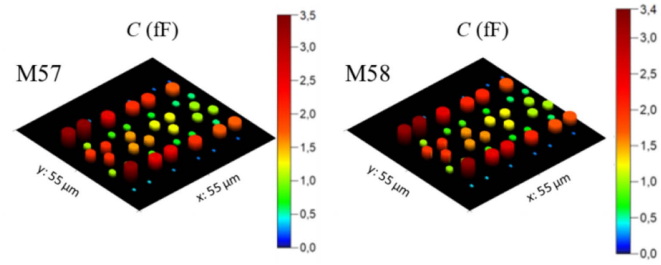

Figure 9. Calibrated capacitances on two samples M57, M58.

3.2.1. Substitution method The samples M57 and M58 have been positioned very close to the reference calibration kit as shown in figure 8. The SMM is calibrated using the values of the capacitance triplet (C_{09}, C_{21}, C_{40}) previously calculated.

One pattern of each sample (48 capacitances) has been calibrated by repeating 5 times the following measurement cycles:

(i) Single topographic and capacitance image of capacitors (C_{09}, C_{21}, C_{40}) to check the SMM calibration;
(ii) Single topographic and capacitance image of capacitors on M57.

The same calibration process has been applied for M58. The VNA working frequency was unchanged (3.808 6 GHz).

3.2.2. Calibrated capacitances The measured capacitance values have been found ranging from 0.1 fF to 3.1 fF (figure 9) with a combined relative uncertainties varying from 14% to 7% respectively.

Table 5 summarizes capacitance values and corresponding uncertainties for 3 particular capacitors from M57 and M58 samples.

The combined standard uncertainties result from the main uncertainty contributions that are summarized in table 6 for M57 sample (similar values are found for M58 sample). As expected, the largest contribution comes from the SMM calibration uncertainty. This one has been estimated following the same way as described in section 3.1.2. No change of the calibration parameters has been detected from the measurements carried out on the reference pattern. The repeatability levels observed on the measurements of C_{09}, C_{21}, and C_{40} have been found between 0.04% and 0.94%.

In contrast, the repeatability of measurements performed on M57 and M58 samples is less high, ranging from 0.6% to 3.6%. Finally, the uncertainty contribution from parasitic capacitances becomes non negligible for the smallest capacitance, reaching almost 5%.

Table 5. Typical measured capacitances and corresponding combined standard uncertainties for three capacitors of samples M57 and M58.

C values (fF)	M57	M58
High	3.14 ± 0.21	3.13 ± 0.25
Intermediate	0.71 ± 0.06	0.71 ± 0.07
Low	0.15 ± 0.03	0.17 ± 0.03

Table 6. Main uncertainty contributions for 3 values measured on M57 sample: C_{high} (3.14 fF), C_{int} (0.78 fF), C_{low} (0.20 fF).

	C_{high}	C_{int}	C_{low}
Uncertainty budget for C_i		(%)	
Repeatability	2.4	2.7	3.6
SMM calibration	6.3	7.8	13.4
Parasitic capacitances	0.2	0.9	4.5
Stray capacitance	*0.0*	*0.4*	*3.5*
Water meniscus	*0.2*	*0.7*	*2.9*
Combined uncertainty u_{Cm}	6.7	8.3	14.2

3.2.3. Permittivity and dopant concentration The comparison of the capacitance values measured on the 48 capacitors of M_{57} and M_{58} patterns to the calculated values based on FEM method, results in significant deviations. These are found decreasing inversely proportional to the thickness of the dielectric layer, pointing out clearly a non-negligible depletion capacitance of the Si substrate. By considering a relative permittivity of $\varepsilon_{r,Si} = 11.7$ for the silicon substrates [29], the depletion capacitances together with the dopant concentration N_a and the permittivity of the silicon dioxide $\varepsilon_{r,SiO2}$ have been estimated. It should be noted here, in contrast with section 3.1, that the permittivity value may not be known since not used for the SMM calibration.

Let us consider the statistic 'chi square' function

$$X^2 = \sum_{i=1}^{48} (y_i - a - b \cdot x_i)^2, \tag{12}$$

where the terms y_i, a, and b and x_i are given by the following relations:

$$y_i = \left(\frac{A_i}{C_{m,i}} \right), \tag{13}$$

Table 7. Relative permittivity ε_r, dopant concentration N_a and depletion capacitance of same three capacitors of samples M57 and M58 mentioned in table 5.

	M57	M58
ε_r	4.0 ± 0.6	4.1 ± 0.6
N_a (atoms cm^{-3})	$(4.5 \pm 0.5) \cdot 10^{14}$	$(3.9 \pm 0.5) \cdot 10^{14}$
C_d values (fF)		
High	6.22 ± 0.47	5.91 ± 0.44
Intermediate	1.53 ± 0.11	1.42 ± 0.11
Low	0.33 ± 0.02	0.30 ± 0.02

with A_i and $C_{m,i}$ the top electrode area and the measured capacitance of the ith capacitor,

$$a = \sqrt{\frac{kT}{\varepsilon_0 \varepsilon_{r,Si} e^2 N_a}} \text{ and } b = 1/\varepsilon_{r,SiO2}, \tag{14}$$

$$x_i = \frac{d_i}{\varepsilon_0 \cdot f_i(d_i, R_i)}, \tag{15}$$

with $f_i(d_i, R_i) = C_{ox}/C_p$ given by the relation (7).

The least square adjustment (LSA) of X^2 in function of the adjustable parameters a and b leads to N_a and $\varepsilon_{r,SiO2}$ values in the order of $4 \cdot 10^{14}$ atoms cm^{-3} values and 4.0 respectively. The depletion capacitance values are between 0.3 fF and 6.2 fF (table 7).

The combined standard uncertainty corresponding to the relative permittivity (table 7) was estimated from the root sum square of the typical uncertainties on the capacitance measurements u_{Cm}, like those given in table 6, and the typical uncertainties related to the determination of the area u_A and the thickness u_d. The last two uncertainties are composed of the same components reported in table 2, with similar values for the repeatability and AFM calibration. The uncertainty related to the tip profile was calculated by assuming unchanged the apex radius and cone angle of the tip.

The combined standard uncertainties related to both the dopant concentration u_{Na} and depletion capacitance (table 7) are composed of the uncertainties u_{Cm} and u_A.

4. Summary and outlook

The substitution calibration method presented in this paper has shown the capabilities of the SMM to calibrate capacitance of micrometric size capacitors at nanoscale and microwave frequencies with combined standard uncertainties varying from 14% to 7% for capacitances ranging from 0.1 fF to 3.1 fF respectively. This was the first time that calibrated capacitance measurements based on the SOL method, were carried out at nanoscale on capacitors other than those used as reference device to calibrate the SMM. It has been demonstrated that by substituting the reference calibration kit with the capacitors of 'unknown' capacitance, the SMM calibration remains valid and accurate. We have established detailed uncertainty budgets allowing one to estimate combined standard uncertainties while the few SMM-based calibrated capacitance measurements reported so far have given only partial uncertainty estimates. These were found in the order of 10% or more in relative value for capacitances in the order of 1 fF [9–12].

Reducing the uncertainty down to a few percent seems achievable particularly by improving both the AFM measurements of the dimensional parameters of the capacitors and the design of calibration kit capacitors. Extending the capacitance range down to 10 aF or even below while keeping an uncertainty less than 10% requires further efforts to be mainly focused on the parasitic effects due to stray capacitors and water meniscus. It demands to fit the SMM with a fully shielded tip and to carry out electromagnetic modeling works.

As well, it was demonstrated that the nanoscale determination of relative permittivity on capacitors can be possible with an SMM whose calibration is based on the SOL method and on standard capacitances of known permittivity. We have estimated a combined standard uncertainty of 15% in relative value for the permittivity of silicon dioxide $\varepsilon_{r,SiO2}$ from capacitors with a p-type doped silicon substrate not conducting enough to avoid parasitic depletion capacitance. From the expected improvements of SMM capacitance measurements cited above, reducing the relative standard uncertainty in the order of a few percent seems to be possible for the nanoscale permittivity measurements. In meantime we plan to compare our method to the one proposed by Gramse *et al* [9] based on the use of tip–sample approach curves. With this method, the authors have measured $\varepsilon_{r,SiO2}$ with a relative uncertainty in the order of 20%.

Acknowledgments

The authors would like to thank Johannes Hoffmann for fruitful discussions about the SMM calibration method. This research work is carried in the framework of the ADVENT project (Grant No. 16ENG06 ADVENT) which is supported by the European Metrology Programme for Innovation and Research (EMPIR). The EMPIR initiative is co-funded by the European's Horizon 2020 research and innovation programme and the EMPIR Participating States.

ORCID iD

François Piquemal https://orcid.org/0000-0002-7950-0475

References

[1] Ekanayake S R, Cortie M B and Ford M J 2004 Design of nanocapacitors and associated materials challenges *Curr. Appl. Phys.* **4** 250–4
[2] Sicard E 2017 Introducing 10-nm FinFET technology in Microwind *HAL Id hal-01558775*
[3] ITRS 2015 Metrology *Int. Technol. Roadmap Semicond. 2.0*

[4] Li L J *et al* 2012 Three-dimensional AlZnO/Al2O3/AlZnO nanocapacitor arrays on Si substrate for energy storage *Nanoscale Res. Lett.* **7** 1–12

[5] Chang S W, Oh J, Boles S T and Thompson C V 2010 Fabrication of silicon nanopillar-based nanocapacitor arrays *Appl. Phys. Lett.* **96** 153108

[6] Wei L *et al* 2016 Low-cost and high-productivity threedimensional nanocapacitors based on stand-up ZnO nanowires for energy storage *Nanoscale Res. Lett.* **11** 213

[7] Son J Y, Shin Y H, Kim H and Jang H M 2010 NiO resistive random access memory nanocapacitor array on graphene *ACS Nano* **4** 2655–8

[8] Shin C *et al* 2013 Fast, exact, and non-destructive diagnoses of contact failures in nano-scale semiconductor device using conductive AFM. *Sci. Rep.* **3** 6

[9] Gramse G, Kasper M, Fumagali L, Hinterdorfer P and Kienberger F 2014 Calibrated complex impedance and permittivity measurements with scanning microwave microscopy *Nanotechnology* **25** 145703

[10] Huber H P *et al* 2010 Calibrated nanoscale capacitance measurements using a scanning microwave microscope *Rev. Sci. Instrum.* **81** 113701

[11] Hoffmann J, Wollensack M, Zeier M, Niegemann J and Huber H 2012 a calibration algorithm for nearfield scanning microwave microscopes *12th IEEE Int. Conf. Nanotechnol. IEEE-NANO* pp 1–4

[12] Dargent T *et al* 2013 An interferometric scanning microwave microscope and calibration method for sub-fF microwave measurements *Rev. Sci. Instrum.* **123705** 1–7

[13] Hommel S, Killat N, Altes A, Schweinboeck T and Kreupl F 2017 Microelectronics reliability determination of doping type by calibrated capacitance scanning microwave microscopy *Microelectron. Reliab.* **76–77** 218–21

[14] Buchter A *et al* 2018 Scanning microwave microscopy applied to semiconducting GaAs structures *Rev. Sci. Instrum.* **89**

[15] Biagi M C, Badino G, Fabregas R, Gramse G, Fumagalli L and Gomila G 2017 Direct mapping of the electric permittivity of heterogeneous non-planar thin films at gigahertz frequencies by scanning microwave microscopy *Phys. Chem. Chem. Phys.* **19** 3884–93

[16] Wu S and Yu J J 2010 Attofarad capacitance measurement corresponding to single-molecular level structural variations of self-assembled monolayers using scanning microwave microscopy *Appl. Phys. Lett.* **97** 1–4

[17] Oladipo A O, Kasper M, Lavdas S, Gramse G, Kienberger F and Panoiu N C 2013 Three-dimensional finite-element simulations of a scanning microwave microscope cantilever for imaging at the nanoscale *Appl. Phys. Lett.* **103** 213106

[18] Wang F *et al* 2014 Quantitative impedance characterization of sub-10 nm scale capacitors and tunnel junctions with an interferometric scanning microwave microscope *Nanotechnology* **25** 405703

[19] Haddadi K, Brillard C, Dambrine G and Theron D 2016 Sensitivity and accuracy analysis in scanning microwave microscopy *IEEE MTT-S Int. Microw. Symp. Dig.* **2016** 1–4

[20] Sassine G *et al* 2017 Memristor device characterization by scanning microwave microscopy *2017 Int. Conf. Manip. Autom. Robot. Small Scales* September pp 1–4

[21] Kasper M, Gramse G and Kienberger F 2017 An advanced impedance calibration method for nanoscale microwave imaging at broad frequency range *IEEE Trans. Microw. Theory Tech.* **65** 2418–24

[22] Haddadi K, Polovodov P, Théron D and Dambrine G 2018 quantitative error analysis in near-field scanning microwave microscopy *MARSS 2018 - Int. Conf. Manip. Autom. Robot. Small Scales* pp 3–6

[23] Khan M S, Séron O, Thuillier G, Thévenot O, Gournay P and Piquemal F 2017 Development of a programmable standard of ultra-low capacitance values *Rev. Sci. Instrum.* **88** 055109

[24] Tuca -S-S, Kasper M, Kienberger F and Gramse G 2017 Interferometer scanning microwave microscopy : *IEEE Trans. Nanotechnol.* **16** 991–8

[25] JCGM 2008 Evaluation of measurement data — guide to the expression of uncertainty in measurement *JCGM 100*

[26] Nečas D and Klapetek P 2011 Gwyddion: an open-source software for SPM data analysis *Cent. Eur. J. Phys.* **10** 181–8

[27] MC2-Technologies 2019 SMM calibration kit

[28] Kazimierczuk M K 2016 *Pulse-Width Modulated DC–DC Power Converters* Second edn (Chichester: John Wiley & Sons, Ltd) (https://doi.org/10.1002/9780470694640)

[29] Robertson J 2004 High dielectric constant oxides *Eur. Phys. J. Appl. Phys.* **28** 265–91

[30] Sze S M and Ng K K *Physics of Semiconductor Devices* Third edn (Hoboken, New Jersey: John Wiley & Sons, Inc.)

[31] BIPM 2019 *Le Système international d'unités - The International System of Units*, 9th edition

[32] Sloggett G J, Barton N G and Spencer S J 1986 Fringing fields in disc capacitors *J. Phys. A. Math. Gen.* **19** 2725–36

[33] CODATA 2019 CODATA Rercommended values of the fundamental physical constants: 2018 NIST SP 961

[34] Janezic M D, Arz U, Begley S, Bartley P, Technologies A and Rosa S 2009 Improved permittivity measurement of dielectric substrates by use of the te111 mode of a split-cylinder cavity *73rd ARFTG Microw. Meas. Conf.* pp 1–3

[35] Haenssler O 2014 Integration of a scanning microwave microscope and a scanning electron microscope: towards a new instrument to imaging, characterizing and manipulating at the nanoscale *2014 Int. Conf. on Manipulation, Manufacturing and Measurement on the Nanoscale (3M-NANO)*

[36] Fumagalli L, Ferrari G, Sampietro M, Casuso I and Mart E 2006 Nanoscale capacitance imaging with attofarad resolution using ac current sensing atomic force microscopy *Nanotechnology* **17** 4581